# FAST Model Calibration and Validation of the OC5-DeepCwind Floating Offshore Wind System Against Wave Tank Test Data

## Preprint

Fabian Wendt, Amy Robertson, Jason Jonkman
*National Renewable Energy Laboratory*

*Presented at the 27th International Ocean and Polar Engineering Conference*
*San Francisco, California*
*June 25–30, 2017*

**NREL is a national laboratory of the U.S. Department of Energy**
**Office of Energy Efficiency & Renewable Energy**
**Operated by the Alliance for Sustainable Energy, LLC**

This report is available at no cost from the National Renewable Energy Laboratory (NREL) at www.nrel.gov/publications.

**Conference Paper**
NREL/CP-5000-68080
July 2017

Contract No. DE-AC36-08GO28308

**NOTICE**



This report is available at no cost from the National Renewable Energy Laboratory (NREL) at www.nrel.gov/publications.

Available electronically at SciTech Connect http:/www.osti.gov/scitech

Available for a processing fee to U.S. Department of Energy and its contractors, in paper, from:

U.S. Department of Energy
Office of Scientific and Technical Information
P.O. Box 62
Oak Ridge, TN 37831-0062
OSTI http://www.osti.gov
Phone: 865.576.8401
Fax: 865.576.5728
Email: reports@osti.gov

Available for sale to the public, in paper, from:

U.S. Department of Commerce
National Technical Information Service
5301 Shawnee Road
Alexandria, VA 22312
NTIS http://www.ntis.gov
Phone: 800.553.6847 or 703.605.6000
Fax: 703.605.6900
Email: orders@ntis.gov

*Cover Photos by Dennis Schroeder: (left to right) NREL 26173, NREL 18302, NREL 19758, NREL 29642, NREL 19795.*

NREL prints on paper that contains recycled content.

# FAST Model Calibration and Validation of the OC5-DeepCwind Floating Offshore Wind System Against Wave Tank Test Data

*Fabian F. Wendt, Amy N. Robertson, and Jason M. Jonkman*
National Wind Technology Center, National Renewable Energy Laboratory
Golden, CO, USA

## ABSTRACT

During the course of the Offshore Code Comparison Collaboration, Continued, with Correlation (OC5) project, which focused on the validation of numerical methods through comparison against tank test data, the authors created a numerical FAST model of the 1:50-scale DeepCwind semisubmersible system that was tested at the Maritime Research Institute Netherlands ocean basin in 2013. This paper discusses several model calibration studies that were conducted to identify model adjustments that improve the agreement between the numerical simulations and the experimental test data. These calibration studies cover wind-field–specific parameters (coherence, turbulence), hydrodynamic and aerodynamic modeling approaches, as well as rotor model (blade-pitch and blade-mass imbalances) and tower model (structural tower damping coefficient) adjustments. These calibration studies were conducted based on relatively simple calibration load cases (wave only/wind only). The agreement between the final FAST model and experimental measurements is then assessed based on more-complex combined wind and wave validation cases.

KEY WORDS: Floating offshore wind turbine; modeling; validation; FAST; calibration; aerodynamics; hydrodynamics; wind field.

## INTRODUCTION

In 2013, a 1:50-scale model of the DeepCwind semisubmersible floating offshore wind turbine was tested at the Maritime Research Institute Netherlands (MARIN) ocean basin under the direction of the University of Maine. The data from this test campaign was then used in 2015/2016 within the framework of Phase II of the International Energy Agency (IEA) Wind Task 30 Project, also known as OC5 (Offshore Code Comparison Collaboration, Continued, with Correlation). The National Renewable Energy Laboratory (NREL), both led and participated in the OC5 project, which included conducting a series of model calibration studies to improve the match between their numerical model and the wave tank test data. Several of these studies and their key findings are presented in this paper. The authors modeled the DeepCwind system using NREL's open-source wind turbine simulation software FAST version 8 (NREL, 2015).

## MODEL DESCRIPTION

The key properties of the numerical and the physical model as tested in the wave tank are summarized below.

### Physical Model Tested in Wave Tank

The system being investigated in this study is the DeepCwind semisubmersible floating wind turbine that was tested at MARIN in 2013 (Helder and Pietersma, 2013), which builds on testing performed for a similar system in 2011.

Fig. 1 illustrates the geometry of the semisubmersible system, which was designed by the University of Maine. The same platform and mooring geometry was also used in the OC4-DeepCwind semisubmersible system examined within the IEA Wind Task 30 Offshore Code Comparison Collaboration Continuation (OC4) project.

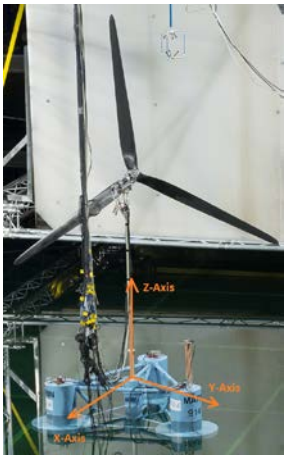


Figure 1. DeepCwind semisubmersible system as tested in MARIN's ocean basin. Positive X along downwind direction. Photo by Andy Goupee, University of Maine

Comparing the OC5 system to the OC4 system, only the turbine changed: the OC4 project and the 2011 wave tank tests used a geometrically scaled version of the NREL 5-MW turbine that did not replicate its thrust and performance, and the 2013 tests and the OC5

project used the MARIN stock wind turbine, which mimics the power, thrust, and torque characteristics of the NREL 5-MW turbine quite well at model scale, but has different airfoil geometries and slightly different scaled-mass properties. The appropriate power and thrust characteristics were achieved through special low-Reynolds-number-specific airfoils in combination with a modified chord-length distribution (Goupee, et al. 2015).

A cable bundle that connects the measurement sensors installed on the floating system to the corresponding data acquisition system is shown in Fig. 1. Prior to every model test, the wave elevation at the future model location was measured without the model present. This undisturbed wave-elevation signal was used as input for the numerical simulations. The wind was generated by an array of fans, followed by a nozzle equipped with guides and stators to achieve a fairly homogeneous, low turbulent wind field (Helder and Pietersma, 2013). MARIN measured the mean wind speed and turbulence intensity distribution for a steady-wind case along the rotor plane of the turbine and found relatively homogeneous spatial distributions of both parameters. The coherence of the wind speed along the rotor plane area was not measured.

The mooring system installed in the 2013 MARIN tests examined here consisted of three equally spaced catenary mooring lines called *BOW*, *PSA*, and *SBA* (Fig. 2). In the MARIN ocean basin, waves propagate from the bottom to top, as shown in Fig. 2. The same mooring system was also used in the OC4-DeepCwind semisubmersible system (Robertson, et al. 2014). According to MARIN and as visible in the test results, some level of hysteresis was present in the mooring system during the tests. This means that the displaced system does not necessarily return to its exact initial position. This hysteresis makes it difficult to assess the surge and sway position measurements because there is a certain level of uncertainty related to the corresponding equilibrium position.

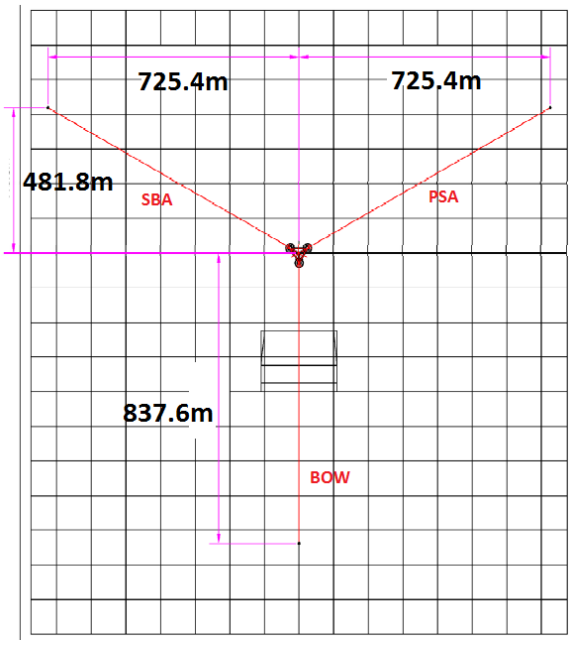


Figure 2. Mooring system as installed (Helder and Pietersma, 2013)

### Numerical FAST Model and Initial Model Calibration

The authors modeled the DeepCwind system tested in the tank at full-scale using FAST v8. All results presented and discussed within this paper refer to full-scale dimensions.

The hydrodynamic platform model uses a hybrid combination of a potential-flow-based approach with additional viscous drag computed via Morison's equation for all submerged members using FAST's hydrodynamics module (HydroDyn). The potential-flow model is based on frequency-dependent wave diffraction excitation and radiation-added mass and damping matrices from WAMIT (WAMIT, Inc. 2013). The HydroDyn model also considers the second-order sum- and difference-frequency wave-excitation loads derived from quadratic transfer functions also computed using WAMIT. The WAMIT model utilized did not include an evaluation of the free-surface integral, which means that the sum-frequency potential term is only approximated here. The transverse and axial member drag coefficients were tuned using measurements from free-decay tests that were performed (the axial drag coefficients were used for the offset base columns, or heave plates). To match the linear damping characteristics of the model during small-amplitude free-decay oscillations, an additional linear damping matrix was included. A summary of the free-decay-based tuning process of the model is given in Wendt, et al. (2016).

Two preloads as well as an additional linear stiffness term in the surge direction, acting on the platform reference point (which is the intersection point of the undisturbed tower-centerline and the free water surface), were introduced to model the potential influence of the measurement cable bundle (whose properties were not measured). The preloads were tuned based on the first regular wave test. For the given regular wave scenario, the introduced preloads were tuned so that the mean mooring-line loads for each fairlead were as close as possible to the measured forces from the experiment (see Wendt, et al. 2016, for a more detailed description). The additional linear stiffness term was tuned to match the surge eigenfrequency. Prior to introducing the additional linear stiffness in surge, the surge eigenfrequency was 10% less than that reported for the model tested in the wave tank.

The dynamic open-source mooring design and analysis software MoorDyn (coupled to FAST) was used to simulate the catenary mooring system. The viscous drag coefficients of the line elements were tuned based on the fairlead load amplitudes from a regular wave test. A detailed description of the mooring system and the corresponding modeling approach that was used by the authors is given in Wendt, et al. (2016).

The utilized mass and stiffness distribution for the tower model are based on a FAST v7 model developed by the University of Maine for the 2011 DeepCwind test campaign. The initial mass distribution was slightly adjusted to match the overall mass and center of mass of the 2013 wave tank model as reported by MARIN. A relatively heavy point mass at the bottom of the tower that represents a six-component measurement frame was removed from the tower mass distribution and added to the lumped platform mass to reduce discontinuities in the tower mass distribution. The initial stiffness distribution also was adjusted to ensure the correct tower bending frequencies, as observed in the wave tank test. An investigation into the appropriate damping parameters for the tower is discussed in a later section. Because the rotor blades of the wave tank model were manufactured using relatively thick layers of carbon fiber, the blades were assumed to be rigid in the FAST model.

## FAST MODEL CALIBRATION STUDIES

This section discusses more extensive calibration studies that were conducted after initial tuning to attempt to improve the agreement between the FAST model and measurements. The term "calibration" as used in this discussion represents the systematic selection of numerical modeling parameters and approaches to improve the match between the FAST simulation and the wave tank test data. Each calibration study was conducted independently.

## Wind Field Calibration

A major uncertainty related to the wave tank tests is the wind field. Prior to the actual test campaign, MARIN investigated the spatial wind field velocity and turbulence intensity distribution through a series of systematic point measurements. During these measurements, all fans were set to a constant rpm value to examine the level of spatial variability of the mean wind speed and turbulence in the wind field. The measurement results are shown below.

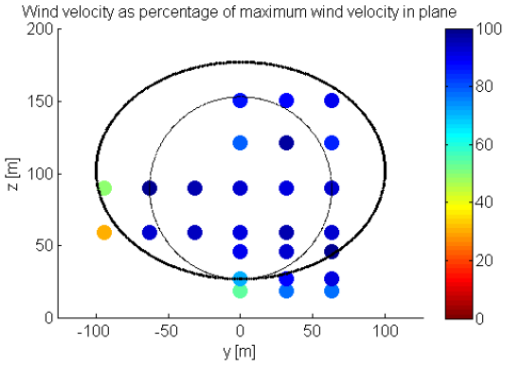


Figure 3. Wind field velocity in the rotor plane of the turbine (Helder and Pietersma, 2013)

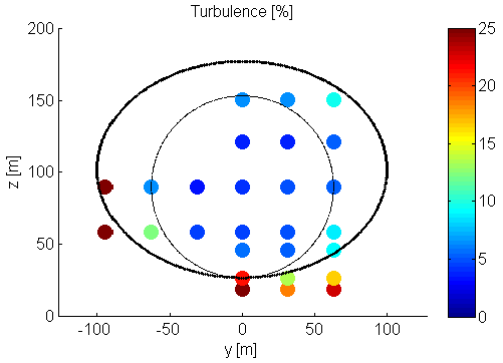


Figure 4. Wind field turbulence intensity in the rotor plane of the turbine (Helder and Pietersma, 2013)

The wind field was found to be relatively homogeneous in terms of mean velocity and turbulence intensity within the rotor disc area. To generate a wind field for the FAST simulations, wind speed measurements in the X- and Z-direction at the location of the hub from a calibration run (without the model present) were used as input for TurbSim (NREL, 2016). Based on the X-component spectra and phases provided by these wind-speed time-series data, TurbSim then generated a full wind field, using the International Electrotechnical Commission (IEC)-61400-3 spatial coherence model (IEC, 2009). This coherence model is intended for use in offshore locations. Whether it captures the coherence characteristics of the model scale experiments conducted in the ocean basin is questionable. However, since no information on coherence was recorded during the experiment, the IEC-61400-3 coherence model is used as a surrogate for this calibration study.
Given the lack of information on the details of the test inflow conditions, spatial coherence was only included for the X velocity component and no spatial coherence was used for the Y and Z velocity components of the wind.

Initial comparisons between the FAST simulations and the MARIN test data for wind-only cases showed several deficiencies in the numerical results. Comparing the tower-base force in the X-direction between the experiment and simulation shows that the simulation generally under-predicts the level of excitation as compared to the experimental test data (Figure 5). The very prominent 3P rotor harmonic also is not captured by the simulation.

During the experiments, no information regarding the spatial coherence was collected. To study the influence of the coherence on the simulation results, a series of wind fields with different levels of coherence was generated. These wind fields were combinations of 100% coherent wind fields and the original wind field that uses the IEC-61400-3 coherence model. The wind field that qualitatively produced the best match with the experimental data in terms of platform pitch and tower-bending response used a weighting factor of 0.17 for the 100% coherent component, and a factor of 0.83 for the corresponding IEC-61400-3 wind field component. The application of these modifications resulted in a wind field with slightly increased coherence as compared to the standard IEC-61400-3 coherence model. To capture the relatively strong 3P response of the model tested in the wave tank, a significant vertical wind shear (power law exponent of $\alpha$=0.2) was introduced to the wind field. The wind field in the wave tank is characterized through a sharp drop in mean wind speed close to the water surface, which justifies the selection of a relatively severe vertical shear exponent for the numerical wind field.

The power spectral density (PSD) of tower-base force signal in the X-direction for two wind-only calibration cases is shown in Figure 5 and Figure 7. The tower-base force signal captures dynamic contributions from the tower vibrations, as well as platform motion–induced load components and excitation forces due to the aerodynamic thrust loads. For the load case with steady wind (Figure 5), the wind field with increased spatial coherence (plotted in red) produces a greater platform pitch and tower-bending response, which falls more in line with what was observed during the wave tank test. The 3P rotor harmonic also is much more pronounced due to the introduced vertical wind shear.

For the load case with dynamic wind (Figure 7), the wind field with increased coherence and vertical wind shear had similar effects, but was slightly less pronounced as compared to the steady wind case. Based on these results, the authors concluded that the modified wind field with increased spatial coherence and vertical wind shear improves the overall agreement between the experiment and simulation.

Steady wind means that all fans were operating with a constant rpm value to generate a wind field with a constant wind speed over time. For dynamic wind fields generated within the experimental campaign the rpm of the fans was varied in order to generate a wind speed spectral distribution as defined by the Norwegian Petroleum Directorate (Helder and Pietersma 2013) measured at the nacelle position.

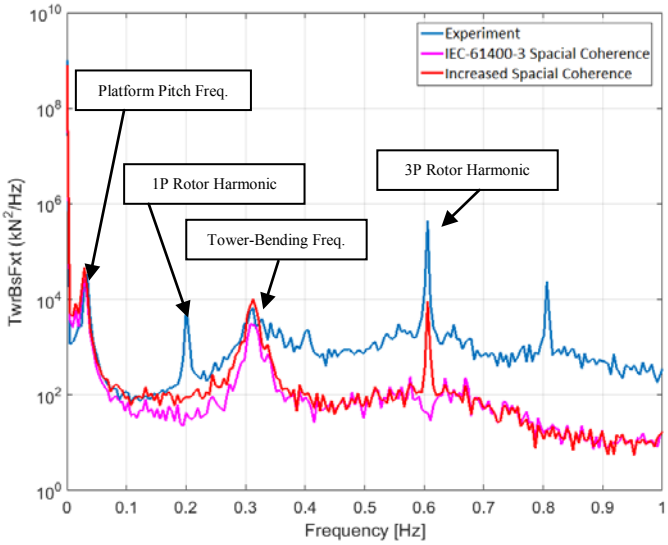


Figure 5. PSD of tower-base force in X-direction for several wind fields, 12.91 m/s steady wind, no waves, 12.13 rpm, 1.22 deg blade pitch

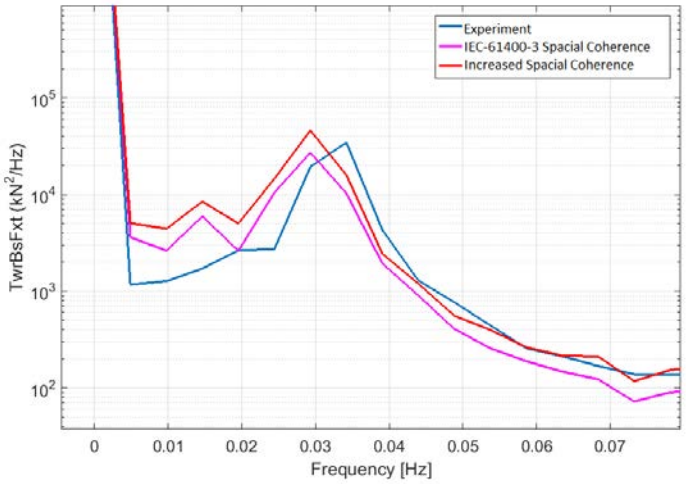


Figure 6. PSD zoom-in on low-frequency region of tower-base force in X-direction for several wind fields, 12.91 m/s steady wind

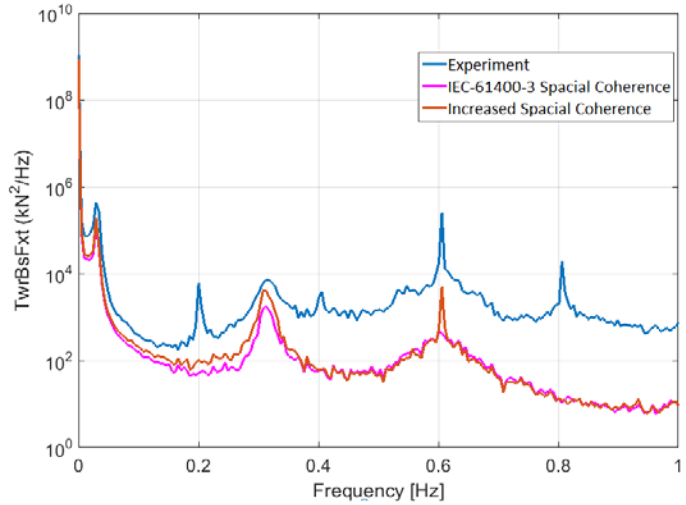


Figure 7. PSD of tower-base force in X-direction for several wind fields, 13.05 m/s dynamic wind, no waves

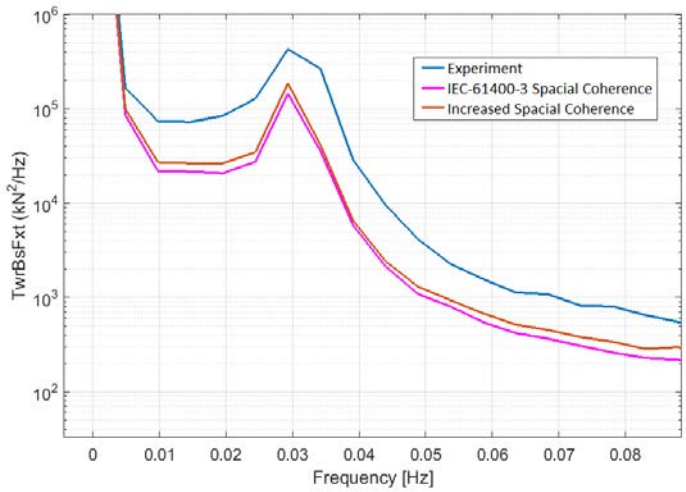


Figure 8. PSD zoom-in on low-frequency region of tower-base force in X-direction for several wind fields, 13.05 m/s dynamic wind, no waves

Next, the authors also investigated the influence of increased turbulence intensity on the simulated system response with the goal of improving the agreement between the experiment and simulation. The standard deviation that directly correlates with the turbulence intensity was multiplied with a factor of 1.25. This adjustment of the standard deviation led to an increased turbulence intensity of 9.4%, as compared to the initial value of 7.5%. The tower-base force in the X-direction was then compared to the system response predicted by the initial simulation for the dynamic wind case (Figure 9). Both simulations used the standard IEC-61400-3 spatial coherence model.

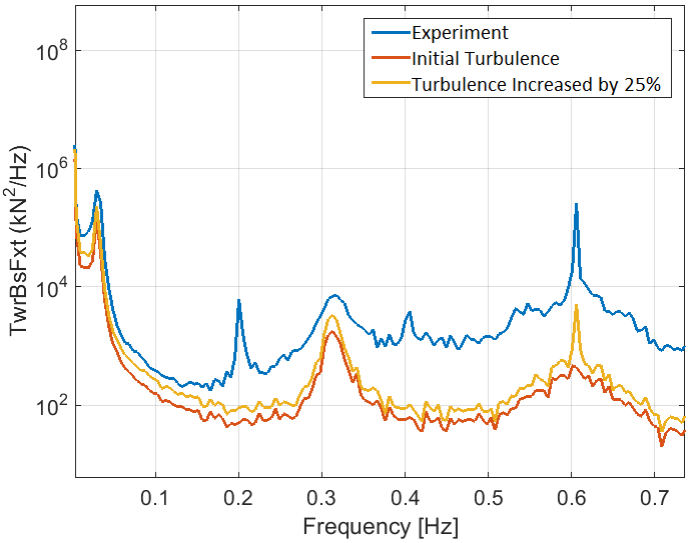


Figure 9. PSD of tower-base force in X-direction for several turbulence levels, 13.05 m/s dynamic wind, no waves

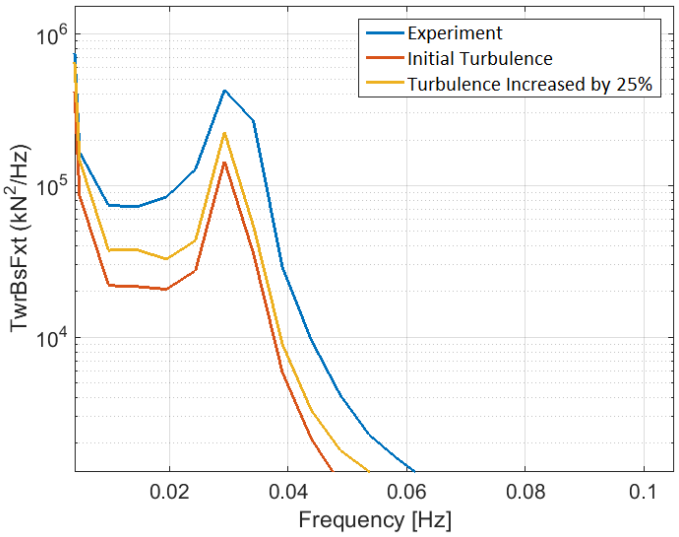


Figure 10. PSD zoom-in on low-frequency region of tower-base force in X-direction for several turbulence levels, 13.05 m/s turbulent wind, no waves

The effect of increased turbulence intensity appears to be very similar to what was observed for wind fields with increased levels of spatial coherence (increased tower bending and pitch response). The globally increased turbulence intensity appears to add some level of broadband frequency excitation throughout the entire frequency range shown in Figure 9, and the increased coherence level mostly influences the low-frequency response of the system. However, the turbulence of the wind field is well known because it is based on the wind-speed measurement data recorded during the experiment. Simply increasing the turbulence with a factor greater than 1.25 to achieve good agreement for the tower-bending and platform pitch response would be a direct deviation from the documented wind conditions during the experiment, which appear quite homogeneous within the rotor plane area (Figure 4). Because increasing the spatial coherence had an effect similar to increasing the global turbulence level, it eventually achieved a better match for tower-bending and platform pitch response with the experimental data. Further, because the coherence was not measured during the experiment, the authors decided to introduce coherence modifications instead of adjusting global turbulence levels to increase the agreement between the simulation and the experiment.

## Aerodynamic Model Calibration

Different combinations of the available airfoil and wake models have been investigated to identify which approach yields the best agreement with the experimental data. The aerodynamic models mainly influence the rotor thrust, therefore the authors focused once more on the tower-base force signal. This signal captures tower vibrations, platform motion–induced load components, and excitation forces due to the aerodynamic thrust loads. Figure 11 illustrates the PSD of the tower-base force in the X-direction for different aerodynamic modeling approaches. *DYNIN* indicates that the simulation uses a generalized dynamic wake model, and *EQUIL* uses an equilibrium wake assumption in accordance with the blade- element-momentum method (Laino and Hansen, 2002). *BEDDOES* indicates that the simulation also uses the Beddoes-Leishman dynamic stall model rather than using the quasi-steady airfoil data.

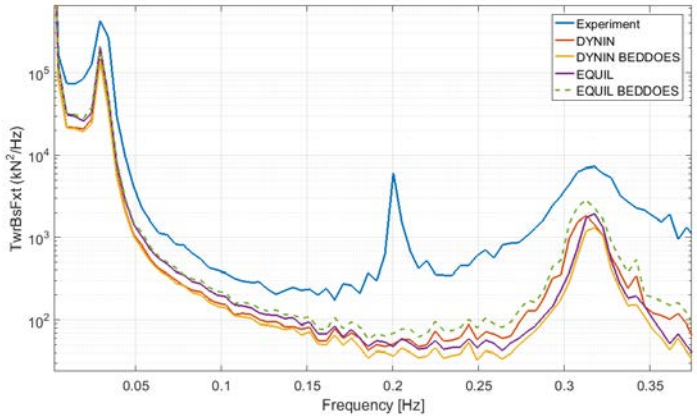


Figure 11. PSD of tower-base force in X-direction for different aerodynamic modeling approaches, 13.05 m/s dynamic wind, no waves

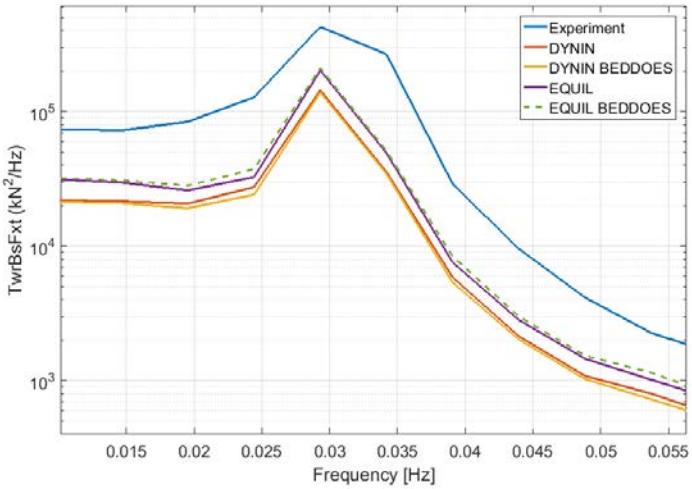


Figure 12. PSD zoom-in on low-frequency region of tower-base force in X-direction for different aerodynamic modeling approaches, 13.05 m/s dynamic wind, no waves

Judging from the results shown in Figure 11, the simulation with the blade-element-momentum approach and the Beddoes-Leishman dynamic stall model (*EQUIL BEDDOES*) produces the results that agree with the experimental data the best. All simulation results are fairly similar, however, and the level of overall observed differences is rather small. Further analysis is required to fully understand the reason for the underestimation of the wind-induced response of the system by the numerical model.

## Rotor Model Calibration

Small errors in blade pitch setting and blade mass are to be expected for every physical turbine model. The authors anticipated potential benefits from including these model deficiencies in the numerical FAST model, especially for the excitation of frequencies related to the rotor harmonics (i.e., 1P, 2P, 3P). Inhomogeneities in terms of blade pitch angle and blade mass were introduced to the rotor of the system and their effect was assessed based on the tower-force PSD in the X-direction (Figure 13).

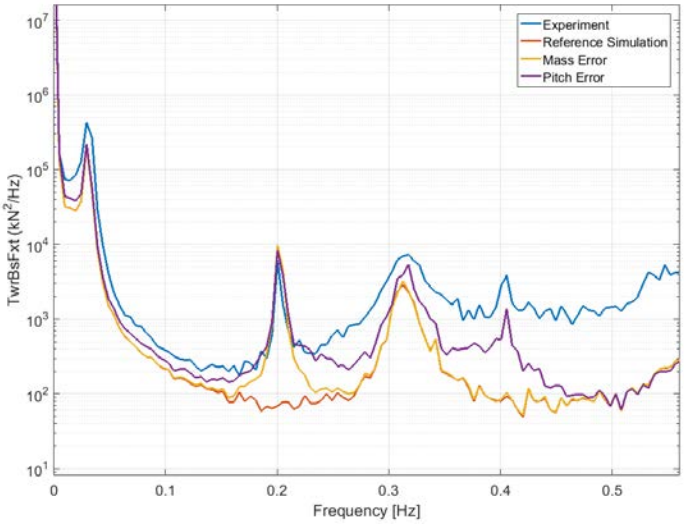


Figure 13. PSD of tower-base force in X-direction for different rotor related inhomogeneities, 13.05 m/s turbulent wind, no waves

*Mass Error* indicates that the individual blade mass for each blade has been altered (Blade 1 +5%, Blade 2 +5%, Blade 3 -10%). *Pitch Error* indicates that the individual blade pitch setting for each blade has been altered (Blade 1: +2 deg, Blade 3: -2 deg).

Both the mass and the blade pitch inhomogeneity clearly have an effect on the response of the system at 0.2 Hz, which coincides with the 1P rotor harmonic frequency. The pitch inhomogeneity also shows a positive effect on the tower-bending response at 0.32 Hz by increasing the system excitation at this frequency. The same positive effect is visible for the model configuration with the blade pitch inhomogeneity at the 2P rotor harmonic frequency (~0.4 Hz), which gets clearly excited because of the introduced pitch error. Based on these findings, the authors decided to introduce the pitch (but not mass) inhomogeneity described above into the system to improve the match with the experimental data.

## Tower Damping Calibration

The tower damping was calibrated based on a wave-only load case. Judging from the response of the simulated system in the tower-bending frequency region (around 0.32 Hz), it was concluded that the tower damping coefficient should be as small as possible without causing any numerical issues. The value finally selected for the structural tower damping is 0.1% of critical damping. The results for the tower-base force in the X-direction for the calibration load case are shown in Figure 14.

The initial tower damping value was set to 2.0%—a value typically used for steel towers (yellow curve). The model with reduced tower damping (red curve) shows an improved approximation of the tower-bending response that was observed in the experiment. The tower-bending response observed during the wave tank test, however, still is underpredicted by the simulation. To avoid any numerical stability issues, the authors refrained from a further reduction of the tower damping coefficient. The reason for the relatively small tower damping that is observed in the physical model is unknown. It potentially could be related to compliance in the connection between the tower base and the platform, which is not included in the FAST model. Additional excitation from the measurement cable could be another explanation for increased excitation of the tower-bending natural frequency.

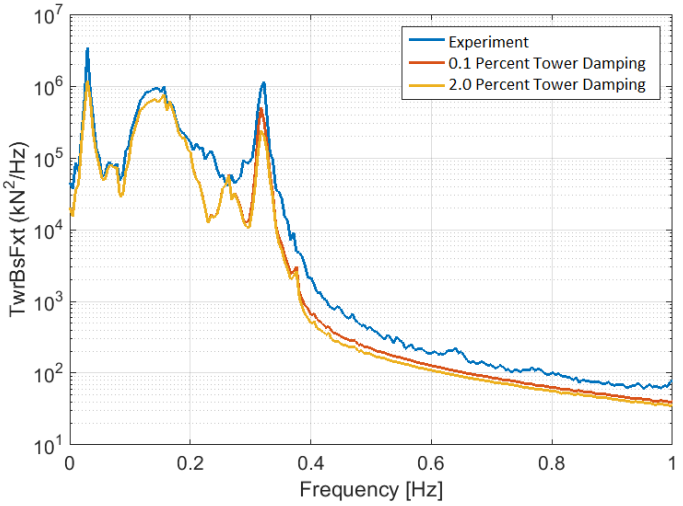


Figure 14. PSD of tower-base force in X-direction for different tower damping coefficients, significant wave height: 7.1 m, peak spectral period: 12.1 s, shape factor: 2.2, JONSWAP spectrum, no wind

## Hydrodynamic Model Calibration

The simulated system response using different hydrodynamic modeling approaches was compared against the experimental data to identify which approach produces the best results. A plot that compares the PSD of the tower-base force in the X-direction for all investigated hydrodynamic modeling approaches is shown in Figure 15.

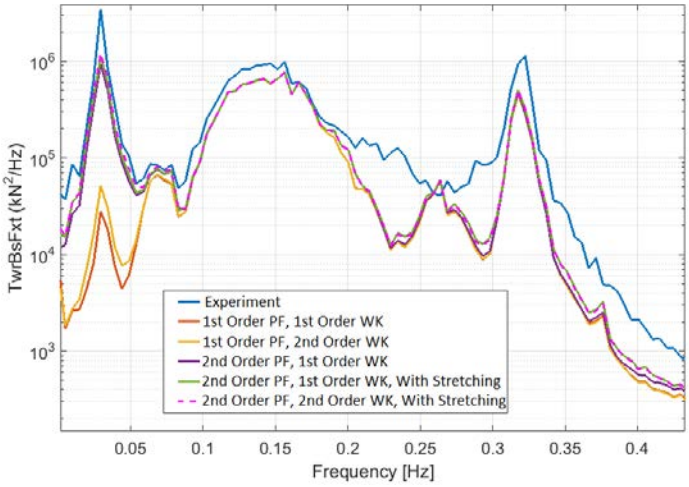


Figure 15. PSD of tower-base force in X-direction for different hydrodynamic modeling approaches, significant wave height: 7.1 m, peak spectral period: 12.1 s, shape factor: 2.2, JONSWAP spectrum, no wind

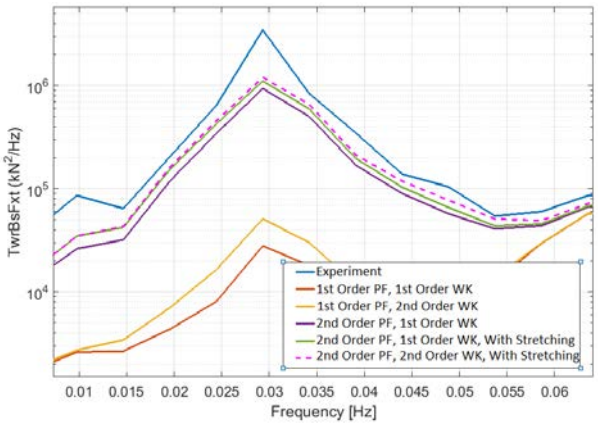


Figure 16. PSD zoom-in on low-frequency region of tower-base force in X-direction for different hydrodynamic modeling approaches, significant wave height: 7.1 m, peak spectral period: 12.1 s, shape factor: 2.2, Jonswap spectrum, no wind

In Figure 15 and Figure 16, "*1st order PF*" indicates that only a first-order WAMIT solution is used for the calculation of the wave-excitation forces; "*2nd order PF*" indicates that second-order sum- and difference-frequency wave-excitation loads are being computed from quadratic transfer functions based on a 2nd order WAMIT solution. "*1st order WK*" indicates linear airy-wave kinematics, and "*2nd order WK*" indicates the use of second-order wave theory as described by Sharma and Dean (Sharma and Dean 1981). The remark *with stretching* indicates the utilization of vertical wave stretching.

Major differences between the different hydrodynamic modeling approaches are evident in the low-frequency region of the tower-base response (Figure 16). The difference-frequency quadratic transfer function (QTF) from the second-order WAMIT solution appears to significantly excite the low-frequency response of the system in the region of the pitch natural frequency (0.03 Hz). Second-order wave kinematics have a similar effect, but are less pronounced than the influence from the second-order WAMIT difference frequency QTF, which could point towards the importance of second-order scattering forces induced by the larger platform members which are only captured through the 2nd order potential flow model. Further investigation (e.g., CFD-based analysis) to assess the observed differences between the numerical model and the experiment is needed.

The authors also explored the utilization of depth-dependent drag coefficients. Smaller drag coefficients at the top of the structure and lesser values at the bottom were specified with the goal of increasing the low-frequency response of the system. The surge and pitch response during regular waves for the model with depth-dependent drag coefficients was compared with the response of the initial model. The comparison showed a modest increase in the low-frequency response of the system, but it was less than when using wave stretching. Additionally, the combination of wave stretching and depth-dependent drag coefficients resulted in less excitation than wave stretching alone. The authors thus decided to not further pursue a depth-dependent distribution of the drag coefficients.

In addition to utilizing the potential flow-based hydrodynamic modeling approach discussed above, the authors also created a hydrodynamic model of the floating platform that is solely based on strip theory using Morison's equation. A comparison of the simulated system response for the potential-flow-based model and the strip-theory-based model is shown below (Figure 17). Second-order wave kinematics were considered for the strip theory model.

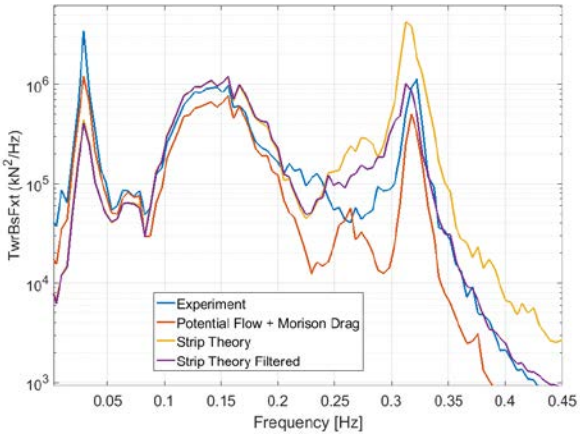


Figure 17. Comparison of tower-base force PSD for strip theory and potential flow theory with Morison drag, significant wave height: 7.1 m, peak spectral period: 12.1 s, shape factor: 2.2, JONSWAP spectrum, no wind

Although the platform pitch response is significantly underpredicted by the strip theory model (0.03 Hz), the tower-bending response (0.32 Hz) is severely overpredicted. Because of the increased tower-bending response of the strip theory model, the authors increased the tower damping from 0.1% of critical damping that was used in the potential flow model (due to underexcitation of that frequency), to 2.0% critical damping for the strip theory model. A significant overprediction of the tower-bending response, however, still is evident (yellow curve in Figure 17), and the authors think it is associated with the invalidity of Morison's long-crested wave assumption for the strip theory model at high frequencies, where the ratio of body diameter and wave length increases beyond a value of 0.2. Considering the dimensions of base and offset columns, the wave frequencies that correspond to this 0.2-ratio threshold are 0.11 Hz and 0.16 Hz, respectively. To address this limitation, the authors introduced a low-pass filter for the wave spectrum. Introducing a low-pass filter at 0.11 Hz/0.16 Hz, however, would truncate a major part of the wave-excitation spectrum. To reach a compromise between the theoretical limitations of the strip theory and the given wave spectrum, the authors decided to introduce a low-pass filter at a frequency of 0.25 Hz. This low-pass-filtered strip theory approach (purple curve in Figure 17) shows significant improvement in terms of agreement with the experimental data, especially at the tower-bending frequency (0.32 Hz).

### White Noise Wave Spectrum Specific Calibration

As described earlier, second-order wave kinematics were found to be beneficial for improving the agreement between the simulation and experiment. One of the wave conditions tested in the ocean basin and examined within the OC5 project uses a white noise wave. Because of the broadband frequency content of a white noise wave spectrum, the initial wave elevation signal measured in the wave tank had to undergo some additional preprocessing prior to using it as input for the second-order wave kinematics model. This is necessary because the second-order calculation assumes that first-order waves are used as input.

In the first step, the measured wave elevation signal from the white noise wave test was directly used as input for a simulation with second-order wave kinematics enabled. The additional spectral energy added by the second-order wave model led to a discrepancy between the measured wave elevation signal from the wave tank test (blue in Figure 18), and the wave elevation signal used in the simulation (red in Figure 18). In the second step, the spectral difference between the signal from the experiment and the initial simulation output was subtracted from

the experimental wave elevation signal. This modified experimental wave elevation signal was then used as input for the final simulation with second-order wave kinematics enabled. The resulting wave elevation spectrum for the final simulation (yellow in Figure 18) shows good agreement with the experimental wave elevation signal.

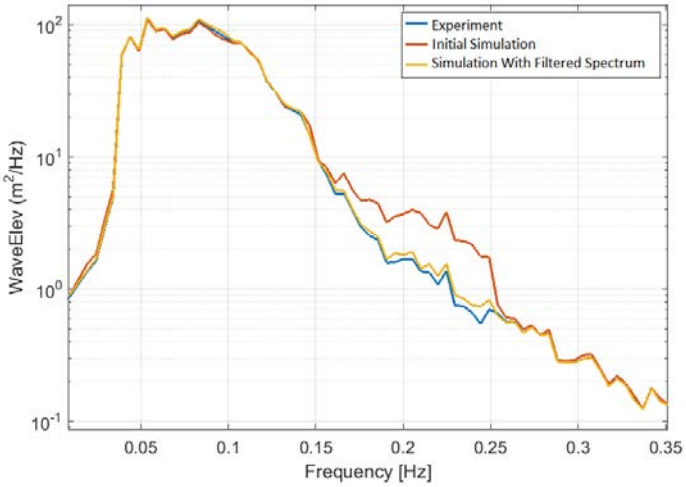


Figure 18. PSD of the white noise wave elevation signal

## SUMMARY OF FINAL MODEL PARAMETERS

The final model configuration selected based on the calibration studies discussed in the previous section is summarized in the table below.

Table 1. Final Configuration of Calibrated Model

| Parameter | Calibrated Setting |
|---|---|
| Wind Field | Uses the measured wind speed time series at hub height. Spatial coherence is a combination of the IEC-61400-3 coherence model (weighting factor 0.83) and a 100% coherence wind field (weight factor 0.17). Introduction of vertical wind shear (power law exponent of α=0.2). |
| Aerodynamic Model | The best agreement between the model and simulation for a turbulent wind field (13.05 m/s) was found using the blade-element-momentum approach together with the Beddoes-Leishman dynamic stall model. |
| Hydrodynamic Model | The best agreement between the simulation and experiment (especially for lower frequencies) was found using second-order wave kinematics in combination with a full, second-order WAMIT QTF and vertical wave stretching. A strip theory model showed significant overprediction of the tower-bending response and significant underprediction of the platform pitch motion. The source for these differences is currently being investigated. |
| Rotor Model | A pitch imbalance was introduced to the model to capture the 1P and 2P rotor harmonic and the relatively large level of excitation at the tower-bending frequency. |
| Tower Damping | A tower damping value of 0.1% critical was used to achieve an appropriate tower-bending response of the system. |

## DISCUSSION OF VALIDATION RESULTS

Following the initial model calibration, the authors ran several combined wind-wave validation cases to examine the agreement between the numerical FAST model in its tuned configuration and the experimental results. The plots of the tower-base force in the X-direction are shown below. The yellow curves shown in Figure 19–22 labeled with "no calibration" show the model configuration with initial tuning only (meaning that the model adjustments discussed in the "FAST MODEL CALIBRATION" section of this paper are not applied here).

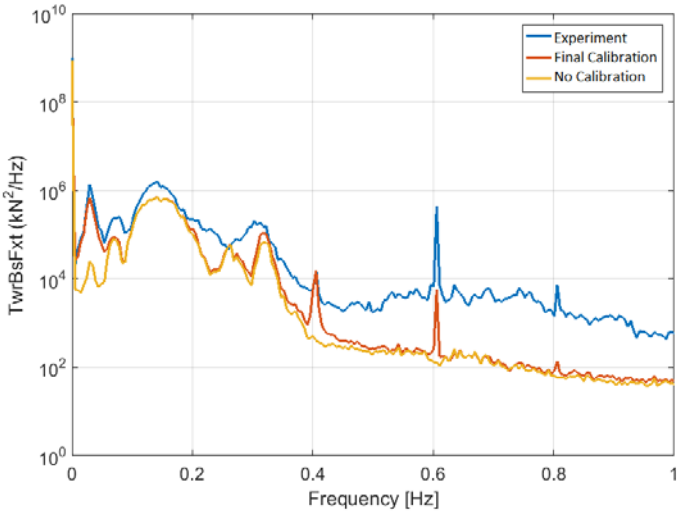


Figure 19. PSD of tower-base force in X-direction, significant wave height: 7.1 m, peak spectral period: 12.1 s, shape factor: 2.2, JONSWAP spectrum, 12.91 m/s steady wind, 1.0 deg blade pitch, 12.1 rpm

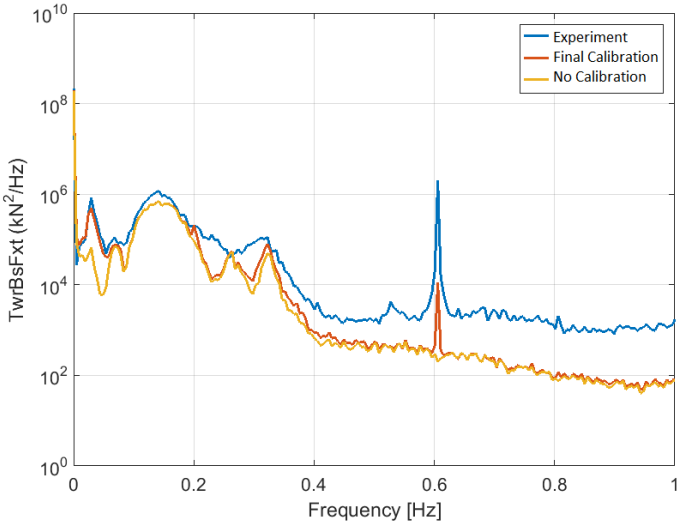


Figure 20. PSD of tower-base force in X-direction, significant wave height: 7.1 m, peak spectral period: 12.1 s, shape factor: 2.2, JONSWAP spectrum, 21.19 m/s steady wind, 17.2 deg blade pitch, 12.1 rpm

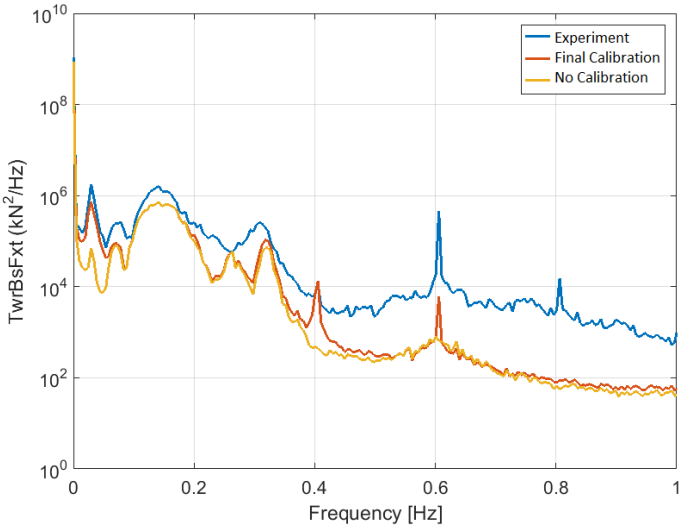


Figure 21. PSD of tower-base force in X-direction, significant wave height: 7.1 m, peak spectral period: 12.1 s, shape factor: 2.2, JONSWAP spectrum, 13.05 m/s dynamic wind, 1.0 deg blade pitch, 12.1 rpm

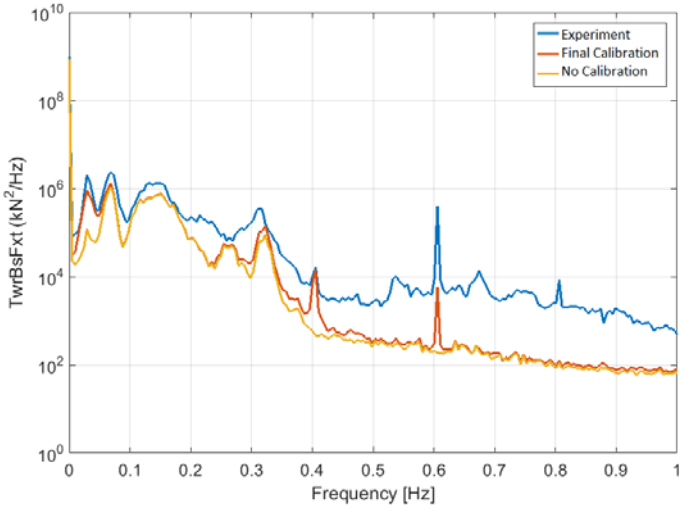


Figure 22. PSD of tower-base force in X-direction, significant wave height: 10.5 m, peak spectral period: 14.3 s, shape factor: 3.0, JONSWAP spectrum, 12.91 m/s steady wind, 1.0 deg blade pitch, 12.1 rpm

Consistent within all examined validation load cases is an underprediction of the response of the system around the pitch natural frequency (0.03 Hz). The simulation results generally appear to underpredict the response of the system for most frequencies between 0 and 1 Hz. The 2P rotor harmonic around 0.4 Hz is approximated relatively well for all load cases with wind speeds of about 13 m/s. For the load case with increased mean wind speed (Figure 20), no significant 2P response is evident in the simulation or experiment. The 3P response that has been introduced through vertical wind shear and blade pitch error is clearly pronounced in the simulation results. The magnitude of this response, however, is significantly less than what was observed in the experiment. The overall tuning that was done for the calibration cases appears to transfer relatively well to the more complex combined wind- and wave-calibration cases.

## CONCLUSIONS

Within the scope of this paper the authors investigated several model adjustments to improve the agreement between numerical FAST simulations and the wave tank test data of a 1:50-scale model of the DeepCwind semisubmersible system, as tested in 2013 at the MARIN wave tank in the Netherlands. Spatial coherence in the wind field was identified as one modeling parameter that was not measured during the experiment but has noticeable effects on the simulation results. Wind fields with different levels of coherence were generated, and the level of spatial coherence generating a system response as close to the experimental data as possible was identified. To identify the approaches yielding the best agreement between numerical simulation and experimental data, the authors also compared different modeling approaches for the hydro- and aerodynamic load calculation. Adjustments in the definition of the rotor (blade pitch and blade mass errors) as well as in the tower model (structural tower damping coefficient) were calibrated to improve the agreement between the simulation and experiment.

Applying all the calibrated model adjustments to the final FAST model of the system enabled the authors to achieve relatively good agreement between simulations and the experiment. An overall underprediction of system response is visible, however, in the simulations for all investigated validation load cases. The source of this general underprediction of the overall system response by the numerical model is still under investigation.

The model calibration work presented within this paper should help to guide future combined wind-wave model scale experiments that are focused on numerical model validation. Quantification of wind field coherence, structural damping and the documentation of uncertainties in the experimental setup (e.g. blade pitch angle, utilized sensor and data acquisition systems) will greatly improve the value of future test campaigns for numerical model validation purposes.

## ACKNOWLEDGMENTS

This work was supported by the U.S. Department of Energy under Contract No. DE-AC36-08GO28308 with the National Renewable Energy Laboratory. Funding for the work was provided by the DOE Office of Energy Efficiency and Renewable Energy, Wind Energy Technologies Office. The authors thank the University of Maine for supplying the MARIN data.



## REFERENCES

Goupee, A, R Kimball, E Ridder, J Helder, A Robertson, and J Jonkman. "A Calibrated Blade-Element/Momentum Theory Aerodynamic Model of the MARIN Stock Wind Turbine." *International Society of Offshore and Polar Engineers Conference (ISOPE).* Kona, HI: National Renewable Energy Laboratory NREL/CP-5000-63568, 2015.

Helder, J, and M Pietersma. *UMAINE–DEEPCWIND/OC4 SEMI FLOATING WIND TURBINE, 27005-1-OB.* Wageningen, NL: MARIN, 2013.

IEC. *61400-3.* Geneva, Switzerland: International Electrotechnical Commission, 2009.

Laino, David J, and Craig A Hansen. *User's Guide to the Wind Turbine Aerodynamics Software AeroDyn.* Salt Lake City, UT, Dec 24, 2002.

NREL. *NWTC Information Portal—TurbSim.* June 14, 2016. https://nwtc.nrel.gov/TurbSim (accessed January 09, 2017).

NREL. *NWTC Information Portal (FAST).* March 19, 2015. https://nwtc.nrel.gov/FAST (accessed January 9, 2017).

Robertson, A, J Jonkman, M Masciola, H Song, A Goupee, A Coulling, C Luan, *Definition of the Semisubmersible Floating System for Phase II of OC4.* Golden, CO: National Renewable Energy Laboratory NREL/TP-5000-60601, 2014.

Sharma, R, and R Dean. "Second-Order Directional Seas and Associated Wave Forces." *Journal of the Society of Petroleum Engineers*, 1981: 4:129–40.

WAMIT, Inc. *WAMIT User Manual Version 7.0.* Chestnut Hill, MA: WAMIT, Inc., 2013.

Wendt, Fabian F, Morten T Andersen, Amy N Robertson, and Jason M Jonkman. "Verification and Validation of the New Dynamic Mooring Modules Available in FAST v8." *26th International Ocean and Polar Engineering Conference.* Rhodes: ISOPE, 2016.